THE JOURNAL OF PHYSICAL CHEMISTRY A
A JOURNAL OF THE AMERICAN CHEMICAL SOCIETY

pubs.acs.org/JPCA

Article

Influence of Molecular Parameters on Rate Constants of Thermal Dissociation/Recombination Reactions: The Reaction System $CF_4 \rightleftarrows CF_3 + F$

Carlos J. Cobos, Elsa Tellbach, Lars Sölter, and Jürgen Troe*

Cite This: J. Phys. Chem. A 2023, 127, 1697−1701

Read Online

ACCESS | Metrics & More | Article Recommendations | Supporting Information

ABSTRACT: The possibilities to extract incompletely characterized molecular parameters from experimental thermal rate constants for dissociation and recombination reactions are explored. The reaction system CF_4 (+M) ⇄ CF_3 + F (+M) is chosen as a representative example. A set of falloff curves is constructed and compared with the available experimental database. Agreement is achieved by minor (unfortunately not separable) adjustments of reaction enthalpy and collisional energy transfer parameters.

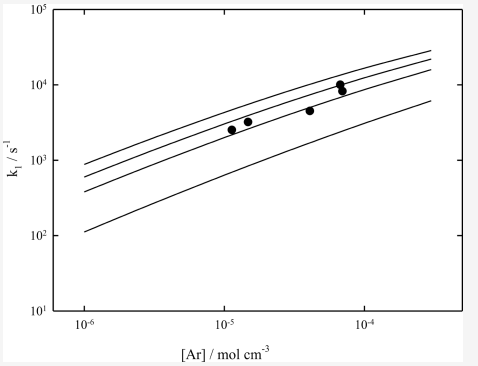

1. INTRODUCTION

Statistical theories of unimolecular reactions have reached a mature state such that they can be used to predict rate constants of thermal dissociation/recombination reactions over a wide range of conditions (see, e.g., refs 1 and 2). Obviously, this is of considerable practical importance. Nevertheless, there are often molecular parameters contributing to the rate constants that are not well known and that require detailed considerations, either by theoretical modeling or by educated guessing. In the following, we demonstrate the influence of selected molecular parameters on the rate constants. Such parameters are the average energy $\langle \Delta E \rangle_{total}$ transferred per collision between the excited molecules and the surrounding bath gas species, characteristic parameters of the potential energy surface (PES) of the reaction system, and, for dissociation reactions in particular, the enthalpy ΔH° of the reaction. These quantities all influence the rate constants, but they do it in different ways. It may not be easy to unravel their respective contributions. This is the issue of the present article.

The dissociation reaction

$$CF_4\ (+M) \rightarrow CF_3 + F\ (+M) \qquad (1)$$

and the reverse recombination reaction

$$CF_3 + F\ (+M) \rightarrow CF_4\ (+M) \qquad (2)$$

are chosen as representative examples (where M stands for an arbitrary partner for collisional energy transfer). The experimental database is limited (for the dissociation reaction 1, see refs 3−5; for the recombination reaction 2, see refs 6−8). We illustrate the influence of the mentioned molecular parameters on the respective rate constants k_1 and k_2, and we try to specify their values by combining experimental and modeling results. Regardless of the precision of the derived parameters, the described approach allows one to construct an internally consistent set of falloff curves and to identify uncertainties of the analysis. In this way, it may help improve recommendations of rate constants (see, e.g., the difference between various experimental results reported in ref 8).

2. MODELING APPROACH

The falloff curves of the rate constants k_1 and k_2 are dominated by limiting low-pressure (subscript 0) and high-pressure (subscript ∞) rate constants. For this reason, attention is first focused on these limiting rate constants. Approximate expressions for the transition of k_1 from $k_{1,0}$ to $k_{1,\infty}$ (or k_2 from $k_{2,0}$ to $k_{2,\infty}$) are available (see, e.g., refs 9−11) and are used when the limiting rate constants have been fixed. Here, we employ the expressions recommended in ref 10, see below.

High-pressure recombination rate constants $k_{2,\infty}$ correspond to rate constants k_{cap} for capture between the combining species. As long as the anisotropy of the PES can be neglected,

Received: January 10, 2023
Revised: January 26, 2023
Published: February 13, 2023

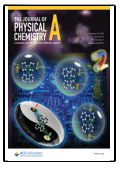

Table 1. Modeled Limiting High-pressure Rate Constants for the Dissociation Reaction $CF_4 \rightarrow CF_3 + F$ ($k_{1,\infty}$) and the Recombination Reaction $CF_3 + F \rightarrow CF_4$ ($k_{2,\infty}$)[a]

T/K	K_{eq}	$k_{2,\infty}^{PST}$	f_{rigid}	$k_{2,\infty}$	$k_{1,\infty}$
300		6.76×10^{13}	1.92×10^{-1}	1.30×10^{13}	
1000	1.31×10^{-25}	7.90×10^{13}	1.74×10^{-1}	1.37×10^{13}	1.80×10^{-12}
2000	1.38×10^{-11}	8.70×10^{13}	1.63×10^{-1}	1.42×10^{13}	1.95×10^{2}
2500	7.81×10^{-9}	8.99×10^{13}	1.59×10^{-1}	1.43×10^{13}	1.12×10^{5}
3000	5.15×10^{-7}	9.23×10^{13}	1.57×10^{-1}	1.45×10^{13}	7.44×10^{6}
4000	8.69×10^{-5}	9.62×10^{13}	1.52×10^{-1}	$.46 \times 10^{13}$	1.27×10^{9}

[a] $k_{1,\infty}$ in s^{-1}, $k_{2,\infty}$ in $cm^3 mol^{-1} s^{-1}$, and equilibrium constant $K_{eq} = k_{1,\infty}/k_{2,\infty}$ in mol cm^{-3}; superscript PST: phase space theory; rigidity factor $f_{rigid} = k_{2,\infty}/k_{2,\infty}^{PST}$, see the text.

k_{cap} is given by phase space theory (PST). For Morse-type PESs, classical trajectory and statistical adiabatic channel calculations in refs 12 and 13 lead to approximate analytical results for k_{cap}^{PST}, which are easily evaluated and show the influence of the Morse parameters β_e, r_e, and D_e in a transparent way. Defining $Y(X) = k_{cap}^{PST} (8\pi kT/\mu)^{-1/2} \beta_e^2$ and $X = \ln(kT/D_e) - \beta_e r_e$, one obtains

$$Y(X) \approx \alpha_0 + \alpha_1 X + \alpha_2 X^2 \quad (3)$$

with the parameters $\alpha_0 = -15.7706$, $\alpha_1 = -8.6364$, and $\alpha_2 = 0.9975$. If recombination from a single electronic level of the reactants into a single electronic state of the adduct is considered, the electronic weight factor f_{el} (given by the relevant ratio of electronic partition functions) has to be multiplied with k_{cap}^{PST} in addition. Table 1 shows results for $k_{cap}^{PST} = k_{2,\infty}^{PST}$ as a function of the temperature T.

Accounting for the anisotropy of the PES reduces $k_{2,\infty}$ to values below $k_{2,\infty}^{PST}$. This is accounted for by a rigidity factor f_{rigid}, which is smaller than unity, that is,

$$k_{2,\infty} = f_{rigid} k_{2,\infty}^{PST} \quad (4)$$

If the anisotropy of the PES is represented by an exponential decay of the frequency $\varepsilon(r)$ [or the frequencies $\varepsilon_i(r)$] of transitional modes along the length r of the forming bond {of the form $\varepsilon(r) \approx \varepsilon(r_e) \exp[-\alpha_e (r - r_e)]$} and if α_e is of the order of 0.5 β_e, according to ref 12, f_{rigid} can be approximated by

$$f_{rigid} \approx 8^{1/2} B_e D_e / [\varepsilon(r_e)]^2 \quad (5)$$

Eq 5 provides a quick access to f_{rigid} and shows its dependence on molecular parameters (B_e here denotes the relevant rotational constant of the forming adduct, see below). It should be noted that the derivation of eq 5 in ref 12 was based on the validity of an approximate relation

$$\alpha_e/\beta_e \approx 0.5 \quad (6)$$

between α_e and β_e. Deviations from eq 5 of less than about ±10% were observed when α_e/β_e differed from 0.5 by less than ±10%. Anisotropies characterized by eq 6 initially were suggested by the analysis of experimental results, see ref 14. Quantum chemical calculations, meanwhile, often confirmed the validity of this relationship (see also the results for the present reaction system shown in the Supporting Information). While the dependence of $k_{2,\infty}$ on details of the PES is only weak, this is different for the limiting high-pressure rate constant $k_{1,\infty}$. As $k_{1,\infty}$ follows from $k_{2,\infty}$ through the equilibrium constant $K_{eq} = k_{1,\infty}/k_{2,\infty}$ and as K_{eq} and $k_{1,\infty}$ both contain the strongly temperature-dependent Boltzmann factor $\exp(-\Delta H_0^\circ/kT)$, the analysis of $k_{1,\infty}$ can be used to determine ΔH_0°. Table 1 compares calculated temperature dependences of $k_{1,\infty}$ and $k_{2,\infty}$, $k_{1,\infty}^{PST}$ and $k_{2,\infty}^{PST}$, as well as the corresponding thermal rigidity factors f_{rigid} (the used molecular parameters of the calculations are given in the Supporting Information).

The calculation of limiting low-pressure rate constants $k_{1,0}$ and $k_{2,0}$ has been described in detail in ref 11 and is not reproduced here. $k_{1,0}$ has been expressed in the form

$$k_{1,0} \approx [M] \beta_c Z_{LJ} \{\rho_{vib,h}(E_0) kT/Q_{vib}\} \exp(-E_0/kT) F_{anh} F_E F_{rot} \quad (7)$$

with various contributions characterized by individual factors. Table 2 shows calculations of such factors (the critical energy

Table 2. Contributing Quantities to Equation 7 for Limiting Low-pressure Rate Constants of the Recombination Reaction $CF_3 + F$ (+He) → CF_4 (+He) at 300 K [[a]in $cm^3 mol^{-1} s^{-1}$, [b]in (kJ mol^{-1})$^{-1}$, [c]Collision Efficiency β_c Calculated with $-\langle\Delta E\rangle_{total}/hc = 100$ cm^{-1}; [d]in $cm^6 mol^{-2} s^{-1}$; Equation 7 from Reference 11]

quantity in eq 7	value
Z_{LJ}[a]	2.58×10^{14}
Q_{vib}	1.54
$\rho_{vib,h}(E_0)$[b]	7.54×10^{8}
F_{anh}	1.79
F_E	1.03
F_{rot}	15.5
β_c[c]	0.24
$k_{rec,0}/[He]$[d]	1.54×10^{21}

E_0 here is identified with ΔH_0°; temperature-dependent quantities are given for 300 K. While the calculation of most of the factors is straightforward and shows the dependence on molecular parameters in a transparent manner, the rotational factor F_{rot} requires attention. It depends on the centrifugal barriers $E_0(J)$ of the system and, hence, on properties of the PES like the rotational constant of the system along the dissociating bond (see the Supporting Information). Properties of collisional energy transfer enter through the overall Lennard-Jones collision frequency Z_{LJ} and a collision efficiency β_c. Information on the latter quantity can be derived from the analysis of experimental values of $k_{1,0}$ and $k_{2,0}$ and is of particular importance. Through the solution of simplified master equations, a relation between β_c and the average (total) energy $\langle\Delta E\rangle_{total}$ of the form

$$-\langle\Delta E\rangle_{total}/F_E kT \approx \beta_c/(1 - \beta_c^{1/2}) \quad (8)$$

was derived (see refs 11 and 15; F_E corrects for the used expression of the energy dependence of the vibrational density

https://doi.org/10.1021/acs.jpca.3c00011
J. Phys. Chem. A 2023, 127, 1697−1701

of states $\rho_{vib,h}(E)$; F_E in general is not far from unity; it should be noted that $\langle\Delta E\rangle_{total}$ differs from the average energy transferred per down-transition, $\langle\Delta E\rangle_{down}$, and the two quantities are related by $\langle\Delta E\rangle_{total} \approx -\langle\Delta E\rangle_{down}^2/(\langle\Delta E\rangle_{down} + F_E kT)$ such that $\beta_c \approx [\langle\Delta E\rangle_{down}/(\langle\Delta E\rangle_{down} + F_E kT)]^2$, see ref 15). Table 2 includes values of β_c estimated with a value of $-\langle\Delta E\rangle_{total}/hc = 100$ cm^{-1}; later on, $\langle\Delta E\rangle_{total}$ will be used as an empirical fit parameter to be extracted from those experiments that are sensitive to $k_{1,0}$ and $k_{2,0}$.

Falloff curves connecting the limiting low- and high-pressure rate constants primarily are expressed in the Lindemann–Hinshelwood form; however, additionally accounting for a broadening of the falloff curves

$$k/k_\infty = \{x/(1 + x)\}F(x) \quad (9)$$

where $x = k_{1,0}/k_{1,\infty}$ or $x = k_{2,0}/k_{2,\infty}$ are proportional to [M] such that x represents a reduced pressure scale. Broadening factors $F(x)$ (being smaller than unity) here are approximated in the form recommended in refs 9–11. The deviations of the falloff curves from the Lindemann–Hinshelwood form are most pronounced near the center of the curves, that is, close to those values of [M] where $k_{1,0}$ is equal to $k_{1,\infty}$ (or where $k_{2,0}$ is equal to $k_{2,\infty}$). The corresponding center broadening factors F_{cent} can be estimated using the methods outlined in refs 9–11 and 16. They can be related to effective numbers of oscillators of the system, but they also contain energy transfer contributions. Symmetric broadening factors $F(x) = F(1/x)$ of the form

$$\log F(x) = \{1/[1 + (\log x/N)^2]\}\log F_{cent} \quad (10)$$

with $N = 0.75–1.27 \log F_{cent}$ from ref 11 often are sufficient for applications, but refined asymmetric expressions

$$F(x) = (1 + x)/[(1 + x^n)]^{1/n} \quad (11)$$

with $n = [\ln 2/\ln(2/F_{cent})]\,[0.8 + 0.2x^q]$ and $q = (F_{cent} - 1)/\ln(F_{cent}/10)$ have also been tested (see refs 9 and 10).

F_{cent} has strong collision (for $\beta_c = 1$) and weak collision ($\beta_c < 1$) contributions, that is, $F_{cent} = F_{cent}^{sc}F_{cent}^{wc}$, with F_{cent}^{sc} as given above (from refs 9–11 and 16) and $F_{cent}^{wc} = \max(\beta_c^{0.14}, 0.64)$ from ref 9. F_{cent} first increases with temperature, and then, it decreases again. Representative values for the present system (with M = Ar) are $F_{cent} \approx 0.74$, 0.17, 0.095, 0.084, and 0.089 for T/K = 300, 1000, 2000, 3000, and 4000, respectively. Obviously, the values of the limiting rate constants are more important for the construction of the falloff curves than the precise values of F_{cent}. Table 3 summarizes the derived values of $k_{1,0}$, $k_{1,\infty}$, $k_{2,0}$, and $k_{2,\infty}$, together with the corresponding K_{eq} and approximate values for F_{cent}.

3. EVALUATION OF EXPERIMENTAL RESULTS

The comparison of experimental results with modeled falloff curves such as that described in Section 2, on one hand, validates the used molecular parameters of the system entering the given analysis. On the other hand, it allows one to locate the experimental rate constants at their proper position along the falloff curves. We illustrate this with the available experimental data for reactions 1 and 2. The rate constant k_2 in the bath gas Ar was first measured in ref 7 at room temperature and at [Ar] = 1.1 × 10^{-7} and 3.7 × 10^{-7} mol cm^{-3}. As an increase of the measured k_2 by about a factor of 4 has been observed, the recombination reaction was assumed to be near its third-order range. The comparison of the data with modeled falloff curves from the present work in Figure 1, however, casts doubt on this interpretation of the measurements. Nevertheless, the measured absolute value of $k_2 = 2.6$ (±0.7) × 10^{13} cm^3 mol^{-1} s^{-1} at [Ar] = 3.7 × 10^{-8} mol cm^{-3} appears roughly reconcilable with the present calculated value of $k_{2,\infty} = 1.3 \times 10^{13}$ cm^3 mol^{-1} s^{-1}. Meanwhile, the modeling predicts a weaker dependence on [M] than that claimed for the experiments. Indeed, the later measurements of refs 6 and 8 (in He between 3.9 × 10^{-8} and 3.8 × 10^{-7} mol cm^{-3}) showed weaker pressure dependences than that found in ref 7. Figure 2 compares the corresponding results with a modeled falloff curve for M = He. The remaining differences between the results from refs 6 and 8 cannot be explained by uncertainties in the used molecular parameters, in particular in the used value for $\langle\Delta E\rangle_{total}$. Therefore, the modeled falloff curves of Figures 1 and 2 based on assumed values of $-\langle\Delta E\rangle_{total}/hc = 100$ or of 500 cm^{-1} for M = He or of Ar appear to provide a more reasonable representation of the pressure dependence of k_2. The agreement with the experiments from ref 6 appears quite satisfactory, while the difference from the results from ref 8 calls for a reinterpretation of the assumed mechanism of the experiments.

Table 3. Modeled Limiting High-pressure (Subscript ∞) and Low-pressure (Subscript 0) Rate Constants for the Dissociation Reaction CF_4 (+Ar) → CF_3 + F (+Ar) (k_1, for Temperatures 1000–4000 K) and the Recombination Reaction CF_3 + F (+Ar) → CF_4 (+Ar) (k_2, for Temperatures 300–1000 K)[a]

$k_{1,\infty} = 4.0 \times 10^{16}\,(T/2500\text{ K})^{-1.4}\exp(-66{,}500\text{ K}/T)$ s^{-1}	1000–4000 K
$k_{2,\infty} = 1.4 \times 10^{13}\,(T/800\text{ K})^{0.04}$ cm^3 mol^{-1} s^{-1}	300–1000 K
$k_{1,0}/[\text{Ar}] = 7.8 \times 10^{20}\,(T/2500\text{ K})^{-9.6}\exp(-70{,}000\text{ K}/T)$ cm^3 mol^{-1} s^{-1}	1000–4000 K
$k_{2,0}/[\text{Ar}] = 5.4 \times 10^{20}\,(T/800\text{ K})^{-5.4}\exp(-1160\text{ K}/T)$ cm^6 mol^{-2} s^{-1}	300–1000 K
$F_{cent} \approx \exp(-T/155\text{ K}) + \exp(-T/600\text{ K}) + \exp(-4880\text{ K}/T)$	300–4000 K

[a]Energy transfer was characterized by $-\langle\Delta E\rangle_{total}/hc = 500$ cm^{-1}. Modeled center broadening factors F_{cent} of 0.75, 0.57, 0.39, 0.26, 0.21, and 0.12 at T = 300, 400, 600, 800, 1000, and 2000 K, respectively, were approximated by the given expression.

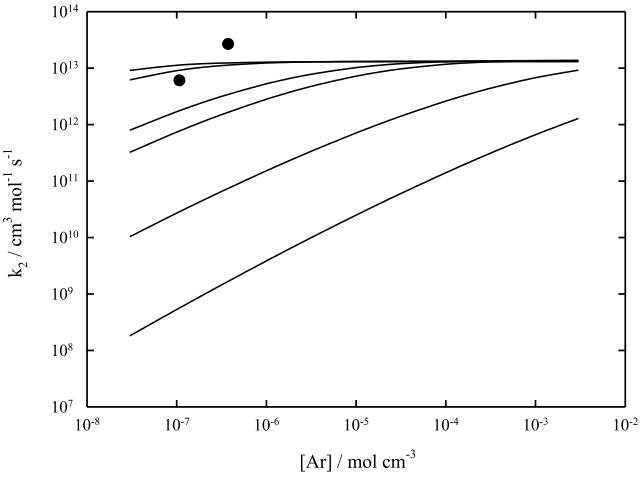

Figure 1. Falloff curves for the recombination reaction CF_3 + F (+Ar) → CF_4 (+Ar) at T = 300, 400, 800, 1000, 2000, and 4000 K (from top to bottom; modeled curves for $-\langle\Delta E\rangle_{total}/hc = 500$ cm^{-1}; experimental points from ref 7).

https://doi.org/10.1021/acs.jpca.3c00011
J. Phys. Chem. A 2023, 127, 1697–1701

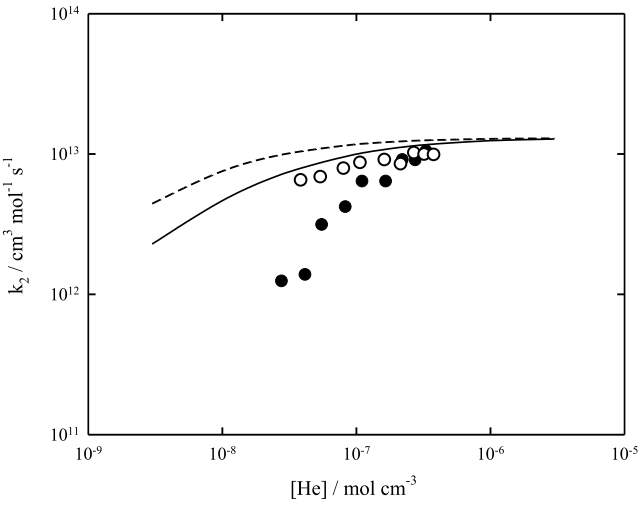

Figure 2. Falloff curve for the recombination reaction CF_3 + F (+He) → CF_4 (+He) at T = 300 K. Solid line: modeled curve using $k_{2,\infty}$ = 1.30 × 10^{13} cm^3 mol^{-1} s^{-1}, $k_{2,0}$/[He] = 1.54 × 10^{21} cm^6 mol^{-2} s^{-1} (calculated with $-\langle\Delta E\rangle_{total}/hc$ = 100 cm^{-1}), and F_{cent} = 0.66. Dashed line: modeled curve using $k_{2,\infty}$ = 1.30 × 10^{13} cm^3 mol^{-1} s^{-1}, $k_{2,0}$/[He] = 3.70 × 10^{21} cm^6 mol^{-2} s^{-1} (calculated with $-\langle\Delta E\rangle_{total}/hc$ = 500 cm^{-1}), and F_{cent} = 0.74. Experimental points: ○ from ref 6 and ● from ref 8.

The question arises how well measured dissociation rate constants k_1 agree with modeling results and whether they provide a further access to molecular parameters. Figure 3

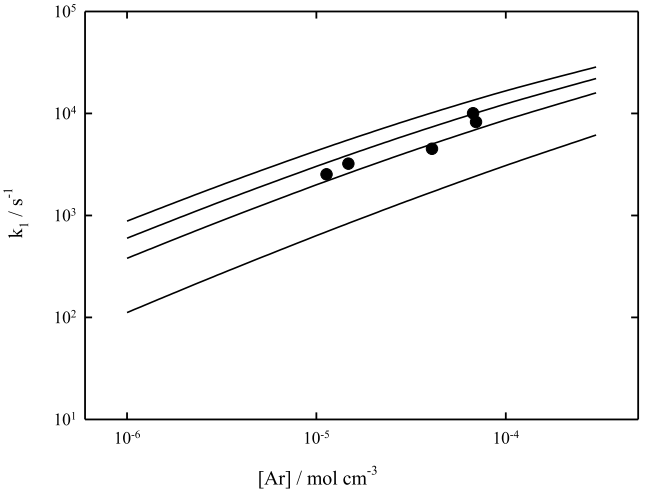

Figure 3. Falloff curves for the dissociation reaction CF_4 (+Ar) → CF_3 + F (+Ar) at T = 2500 K (modeled curves for $-\langle\Delta E\rangle_{total}/hc$ = 100, 500, 1000, and 2000 cm^{-1} from bottom to top, modeling with rate constants $k_{1,0}$ and $k_{1,\infty}$ as well as F_{cent} from Table 3; ●: experimental points from ref 4).

compares measurements of k_1 at T = 2500 K and [Ar] between 10^{-5} and 10^{-4} mol cm^{-3} with modeling results for a series of values of $-\langle\Delta E\rangle_{total}/hc$. The best agreement seems to be obtained with a value of $-\langle\Delta E\rangle_{total}/hc$ of the order of 500 cm^{-1}. Modeling of the temperature dependence of the corresponding falloff curves in Figure 4 clearly confirms that the dissociation measurements have been made far below the high pressure limit of the reaction, while recombination measurements at 300 K were made close to the high pressure limit of the reaction. As the latter thus practically cannot

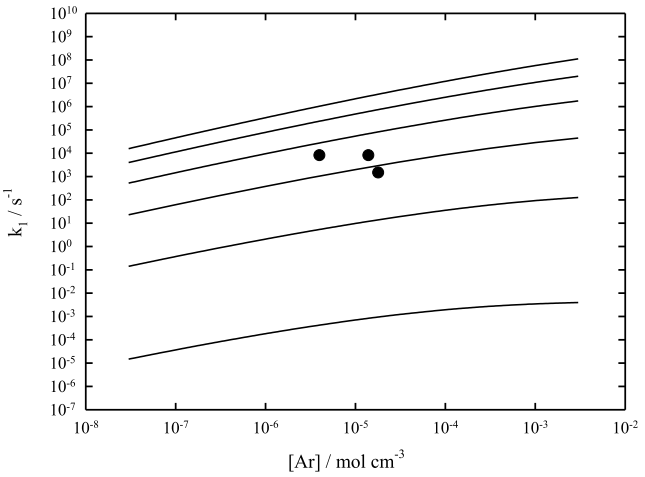

Figure 4. Modeled falloff curves for the dissociation reaction CF_4 (+Ar) → CF_3 + F (+Ar) at the temperatures T = 1500, 2000, 2500, 3000, 3500, and 4000 K (from bottom to top; modeling with rate constants $k_{1,0}$ and $k_{1,\infty}$ as well as F_{cent} from Table 3 and for $-\langle\Delta E\rangle_{total}/hc$ = 500 cm^{-1}; ●: representative experimental points from ref 3 at temperatures between 2400 and 3000 K).

provide an access to $\langle\Delta E\rangle_{total}$, one might be tempted to extract $\langle\Delta E\rangle_{total}$ from Figure 3. However, there is an alternative interpretation. Besides $\langle\Delta E\rangle_{total}$, k_1 in Figure 3 also depends on the precise value of the reaction enthalpy ΔH_0°. Decreasing $-\langle\Delta E\rangle_{total}/hc$ from 500 to 100 cm^{-1} in Figure 3 would decrease the modeled k_1 at [Ar] = 10^{-5} mol cm^{-3} by about a factor of 2.9. This decrease could be compensated by a decrease of ΔH_0° of reaction 1 by about 22 kJ mol^{-1}. As the uncertainty of ΔH_0° apparently is markedly smaller today (see the Supporting Information), it appears more probable that $-\langle\Delta E\rangle_{total}/hc$ in the present case is of the order of 500 cm^{-1}, such as that fitted in Figure 3, although this value is larger than the value of 100 cm^{-1} generally assumed in our modeling. In any case, this example illustrates the sensitivity of the modeled rate constants on molecular parameters. Unfortunately, the thermochemical parameter ΔH_0° and the energy transfer parameter $\langle\Delta E\rangle_{total}$ cannot be separated in the analysis. In particular, no conclusion on the temperature dependence of $\langle\Delta E\rangle_{total}$ for the reaction CF_4 (+Ar) ⇄ CF_3 + F (+Ar) can be drawn. In other cases [e.g., the CH_4 (+Ar) ⇄ CH_3 + H (+Ar) system analyzed in ref 17], only a weak temperature dependence of $\langle\Delta E\rangle_{total}$ was postulated.

4. CONCLUSIONS

Regardless of whether correct molecular parameters have been used in the modeling or not, fixing $\langle\Delta E\rangle_{total}$ and ΔH_0° to the values used for the interpretation of Figure 3 and assuming only a weak temperature dependence of $\langle\Delta E\rangle_{total}$, the corresponding set of modeled falloff curves shown in Figure 4 provides an internally consistent picture of the temperature and pressure dependence of reactions 1 and 2. The outlined procedure illustrates the influence of various molecular parameters on the rate constants, and it may be used to identify problems of the interpretation of experimental results.

■ ASSOCIATED CONTENT

Supporting Information

The Supporting Information is available free of charge at https://pubs.acs.org/doi/10.1021/acs.jpca.3c00011.

https://doi.org/10.1021/acs.jpca.3c00011
J. Phys. Chem. A 2023, 127, 1697−1701

Molecular details of the reaction CF_4 (+M) ⇄ CF_3 + F (+M) (PDF)

AUTHOR INFORMATION

Corresponding Author

Jürgen Troe − *Max-Planck-Institut für Multidisziplinäre Naturwissenschaften, D-37077 Göttingen, Germany; Institut für Physikalische Chemie, Universität Göttingen, D-37077 Göttingen, Germany;* orcid.org/0000-0002-4347-0307; Email: juergen.troe@mpinat.mpg.de

Authors

Carlos J. Cobos − *INIFTA, Facultad de Ciencias Exactas, Universidad Nacional de La Plata, CONICET, CP 1900 La Plata, Argentina*

Elsa Tellbach − *Max-Planck-Institut für Multidisziplinäre Naturwissenschaften, D-37077 Göttingen, Germany; Institut für Physikalische Chemie, Universität Göttingen, D-37077 Göttingen, Germany*

Lars Sölter − *Max-Planck-Institut für Multidisziplinäre Naturwissenschaften, D-37077 Göttingen, Germany; Institut für Physikalische Chemie, Universität Göttingen, D-37077 Göttingen, Germany*

Complete contact information is available at: https://pubs.acs.org/10.1021/acs.jpca.3c00011

Notes

The authors declare no competing financial interest.

ACKNOWLEDGMENTS

Financial support of this work by the Deutsche Forschungsgemeinschaft (Project TR 69/23-1) is gratefully acknowledged.

REFERENCES

(1) Cobos, C. J.; Hintzer, K.; Sölter, L.; Tellbach, E.; Thaler, A.; Troe, J. High-Temperature Fluorocarbon Chemistry Revisited. *J. Phys. Chem. A* **2021**, *125*, 5626−5632.

(2) Cobos, C. J.; Sölter, L.; Tellbach, E.; Troe, J. The Thermal Dissociation-Recombination Reactions of SiF_4, SiF_3, and SiF_2: A Shock Wave and Theoretical Modeling Study. *J. Phys. Chem. A* **2022**, *126*, 8871−8877.

(3) Modica, A. P.; Sillers, S. J. Experimental and Theoretical Kinetics of High-Temperature Fluorocarbon Chemistry. *J. Chem. Phys.* **1968**, *48*, 3283−3289.

(4) Knight, G.; Sölter, L.; Tellbach, E.; Troe, J. Shock wave and modeling study of the reaction CF_4 (+M) ⇔ CF_3 + F (+M). *Phys. Chem. Chem. Phys.* **2016**, *18*, 17592−17596.

(5) Chen, L.; Zhang, B.; Li, X. Decomposition Pathway and Kinetic Analysis of Perfluoroketone $C_5F_{10}O$. *J. Phys. D: Appl. Phys.* **2020**, *53*, 415502.

(6) Plumb, I. C.; Ryan, T. R. Gas-phase reactions of CF_3 and CF_2 with atomic and molecular fluorine: Their significance in plasma etching. *Plasma Chem. Plasma Process.* **1986**, *6*, 11−25.

(7) Butkovskaya, N. I.; Larichev, M. N.; Leipunskii, I. O.; Morozov, I. I.; Talroze, V. I. Mass-Spectrometric Study of the Recombination of Atomic Fluorine with CF_3 Radicals and CF_2 Biradicals. *Kinet. Catal.* **1980**, *21*, 263−267.

(8) Dils, B.; Vertommen, J.; Avondale Carl, S. A.; Vereecken, L.; Peeters, J. The kinetics of the CF_3+ $CF_3$and CF_3+ F combination reactions at 290 K and at He-pressures of ≈1-6 Torr. *Phys. Chem. Chem. Phys.* **2005**, *7*, 1187−1193.

(9) Troe, J.; Ushakov, V. G. Revisiting Falloff Curves of Thermal Unimolecular Reactions. *J. Chem. Phys.* **2011**, *135*, 054304.

(10) Troe, J.; Ushakov, V. G. Representation of "Broad" Falloff Curves for Dissociation and Recombination Reactions. *Z. Phys. Chem.* **2014**, *228*, 1−10.

(11) Troe, J. Predictive Possibilities of Unimolecular Rate Theory. *J. Phys. Chem.* **1979**, *83*, 114−126.

(12) Maergoiz, A. I.; Nikitin, E. E.; Troe, J.; Ushakov, V. G. Classical Trajectory and Statistical Adiabatic Channel Study of the Dynamics of Capture and Unimolecular Bond Fission. IV. Valence Interactions between Atoms and Linear Rotors. *J. Chem. Phys.* **1998**, *108*, 5265−5280.

(13) Maergoiz, A. I.; Nikitin, E. E.; Troe, J.; Ushakov, V. G. Classical Trajectory and Statistical Adiabatic Channel Study of the Dynamics of Capture and Unimolecular Bond Fission. V. Valence Interactions between Two Linear Rotors. *J. Chem. Phys.* **1998**, *108*, 9987−9998.

(14) Cobos, C. J.; Troe, J. Theory of Thermal Unimolecular Reactions at High Pressures. II. Analysis of Experimental Results. *J. Chem. Phys.* **1985**, *83*, 1010−1015.

(15) Troe, J. Theory of Thermal Unimolecular Reactions at Low Pressures. I. Solutions of the Master Equation. *J. Chem. Phys.* **1977**, *66*, 4745−4757.

(16) Troe, J. Theory of Thermal Unimolecular Reactions in the Fall-off Range. I. Strong Collision Rate Constants. *Ber. Bunsenges. Phys. Chem.* **1983**, *87*, 161−169.

(17) Cobos, C. J.; Troe, J. The Dissociation-Recombination System CH_4 + M ⇔ CH_3 + H + M: II. Evaluation of Experiments up to 5000 K and Temperature Dependence of. *Z. Phys. Chem.* **1992**, *176*, 161−171.